Gas permeability and compressive strength evaluation of porous Al_2O_3 supported membrane

F. N. de Mattos[1], A. L. Molisani[1]*, L. Caldeira[1]

[1]Instituto Federal de Educação, Ciência e Tecnologia do Sudeste de Minas Gerais, R. Bernardo Mascarenhas 1283, 36080-001, Juiz de Fora, MG, Brazil

Abstract

The aim was to investigate the feasibility of using a device to characterize permeability in porous substrates with low gas flux. Al_2O_3 supports were prepared by dry pressing using 1 to 3 wt% of polyethylene glycol (PEG) as a pore-forming agent. The green body was partially sintered at 1300 ºC. CO_2 gas was used to measure both the pressure loss and the gas flux passing through the porous substrate. The permeability behavior was analyzed by the Darcy and Forchheimer models. The correlation between Darcy's and Forchheimer's permeabilities showed that the porous substrates may be used as membranes for micro, ultra, and nanofiltration. The mechanical resistance and the gas permeability exhibited antagonistic dependencies in relation to porosity, being identified as an optimized condition at 2 wt% PEG, in which the two properties presented high values.

Keywords: Al_2O_3, porosity, permeability, mechanical property.

INTRODUCTION

Membrane separation processes encompass a wide range of applications, such as pharmaceutical, cosmetic, food, chemical, petrochemical, desalination, and wastewater treatment industries [1-4]. Membranes can be manufactured from polymeric and ceramic materials [1, 5, 6]. Polymeric membranes are more consumed than ceramic membranes, but the consumption of ceramic membranes has been increasing due to the optimization of their properties [1], such as low filter strength, high filtration efficiency, high thermal and chemical stability, long lifetime, good mechanical properties under adverse conditions, and easy cleaning [1-3, 7]. Ceramic membranes may have symmetrical or asymmetric structures [4]. If the structure is symmetrical, the transport properties are constant along the cross-section and so the flux depends on the membrane thickness [8]. Consequently, an asymmetric structure has its transport properties varying along the cross-section, being composed of multilayers with porosity gradient [9]. In the second type of structure, the pore size gradually increases from the upper layer towards the bottom layer of porous support [10]. This porous support can be commonly manufactured by extrusion or pressing with tubular and flat shapes, respectively [11]. On the other hand, different routes can be used to prepare the porous structure, including partial sintering, pore-forming agent, replica template, and direct foaming [12]. It is difficult to control the porous structure since the size and fraction of pores depend on different process parameters, such as ceramic powder's particle size, degree of partial sintering, size, shape, and amount of pore-forming agent and replica structure. In contrast, the directional freezing process of solvent existent in the ceramic slurry (freeze-casting) may result in homogeneous structures with highly interconnected pore networks, which improves the permeability in relation to the aforementioned processes [10, 13].

The porous support must provide mechanical resistance enough to avoid unexpected troubles in operation and, at the same time, must provide low resistance to gas flux [9, 11, 14]. Al_2O_3 powder is the main raw material used in the production of the porous support [15], but other ceramic powders also can be employed, such as TiO_2, SiO_2, ZrO_2, perovskite, mullite, cordierite [10, 16], as well as non-oxide compounds (nitrides, carbides, and borides) [5], and clays [17, 18]. Various processes are used to deposit the thin films onto the porous support, including spin coating, screen printing, and dip coating [19]. The intermediate layers prevent the infiltration of the selective layer into the porous support, as well as provide a smooth, flawless surface for the deposition of the selective layer with controlled porosity [20]. Thus, the nature of the membrane (hydrophobic or hydrophilic) is defined by the composition of the materials used in its manufacture (ceramic powder and thin-film coating), while the application is determined by the pore size [1]. For example, membranes with macropores (>50 nm) and mesopores (2-50 nm) are respectively indicated for the microfiltration and ultrafiltration systems, whereas membranes with pore sizes between 0.2 to 2 nm are employed in nanofiltration systems [1]. Although membranes can be tailored for different applications, there is an open question addressed to operating conditions of low to medium flux [20]. Thus, an experimental apparatus in order to achieve a porous alumina membrane with good agreement between permeability and mechanical resistance was designed. In the present work, the gas permeability behavior of porous Al_2O_3 supports obtained by dry pressing, the addition of pore-forming agent, and partial sintering was investigated.

*https://orcid.org/0000-0003-3827-1853

The aim was to check the feasibility of using the above-mentioned device in the characterization of permeability in porous supports with low gas flux.

MATERIALS AND METHODS

The ceramic support was prepared using Al_2O_3 powder (Alpha Bond) and polyethylene glycol (PEG, molecular weight 6000, Sigma-Aldrich) as a pressing binder and pore-forming agent. Three supports were produced for each PEG content (1, 2, and 3 wt%). The raw materials (Al_2O_3 and PEG) were manually dry mixed and then compacted with uniaxial pressure of around 15 MPa for 5 min. The pressed body, disk shape with 10 mm in thickness and 30 mm in diameter, was heated in an oven at 110 ºC for 5 h. The sintering process was carried out in the air using a furnace (Thermo King) and a heating rate of around 5 °C/min. The sintering process took place in two steps, including the first plateau at 800 ºC for 10 min and a second plateau at 1300 ºC for 30 min, followed by cooling at a rate of around 10 ºC/min.

The sintered body was submitted to the apparent density and apparent porosity determination test based on the ABNT NBR ISO 10545-3:2020 standard. The experimental results were calculated and expressed in terms of relative density (ρ_r), apparent porosity (P_a), total porosity (P_t), and closed porosity (P_c) according to the following equations [21]:

$$\rho_r = \frac{\rho_a}{\rho_t} \cdot 100 \quad (A)$$

$$P_t = 100 - \rho_r \quad (B)$$

$$P_c = P_t - P_a \quad (C)$$

where ρ_a is the apparent density and ρ_t is the theoretical density of Al_2O_3 (3.95 g/cm^3). The microstructural analysis was conducted in a scanning electron microscope (SEM, VEGA3, Tescan), while mechanical resistance was measured in a compression testing machine (WDW 200, Time).

The porous support permeability test was performed in a device made in our laboratory, using CO_2 as a permeation medium (fluid). The porous support was placed in a pressure chamber made of 316L stainless steel (Fig. 1a) and then CO_2 gas was injected as schematically described in Fig. 1b. The inlet and outlet pressures were measured by a pressure gauge in response to the gas flux variation, which was controlled and measured by a needle valve and soap film flowmeter, respectively. The fluid permeated the central region of the porous Al_2O_3 support, which corresponded to 40% of the total area of its cross-section. The CO_2 flux and pressure into the gas line remained constants, whose values were 10 L/min and 6 MPa, respectively. The system was purged with a mechanical vacuum pump before each permeability test. Permeability can be determined as a function of velocity and the pressure drop of a fluid passing through the porous material. If the flux rate is very low, there is a laminar regime and Darcy's law is valid (prevail viscous factors). Darcy's law exhibits a linear relationship between pressure gradient and fluid velocity and, for compressible fluid, Darcy's equation can be expressed as [21, 22]:

$$k_D = \frac{2\,P_m\,\mu.v.L}{P_e^2 - P_S^2} \quad (D)$$

where k_D is the Darcy permeability, P_m is the average value of the inlet (P_e) and outlet (P_s) pressures, μ is the CO_2 gas viscosity (1.5026×10^{-5} Pa.s) [22], v is flux speed (m/s), and L is the porous material thickness. If the regime is turbulent, the inertial factors become more significant [23]. In this case, the Forchheimer equation, which expresses the parabolic dependence of the pressure gradient on the velocity of fluid passing through the porous material, has a more realistic approximation [21, 24]. Forchheimer's equation for compressible fluid can be expressed as [20, 23]:

$$\frac{P_e^2 - P_S^2}{2\,P_m.L} = \frac{\mu}{K_D} v + \frac{\rho}{K_F} v^2 \quad (E)$$

where ϱ is the CO_2 gas density (1.5012 kg/m^3) [22] and k_F is Forchheimer permeability. The dimensionless Forchheimer's number (F_0) is used as a parameter to analyze the contribution of viscous and inertial effects which leads to a decrease in pressure [21, 24]:

$$F_0 = \frac{\rho.v}{\mu} \cdot \frac{k_1}{k_2} \quad (F)$$

The viscous and inertial effects related to the pressure drop of fluid passing through the porous material can be expressed, respectively, in percentage terms by the following equations [20, 24]:

$$E_{viscous}(\%) = \frac{1}{1 + F_0} \quad (G)$$

$$E_{viscous}(\%) = \frac{F_0}{1 + F_0} \quad (H)$$

The average pore diameter (d_p) of the porous support was estimated from Darcy permeability (k_D) and apparent

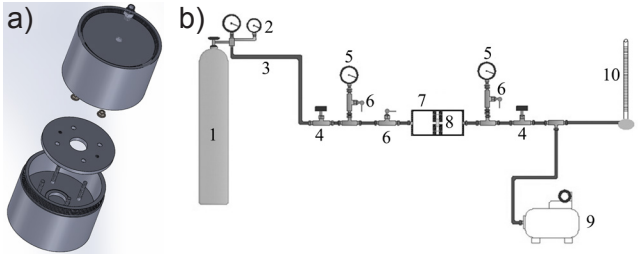

Figure 1: Schematics showing exploded view of the 316L stainless steel pressure chamber (a) and components of the permeate for permeability test (b): 1) CO_2 gas cylinder; 2) pressure gauge to regulate pressure in the gas line; 3) gas line; 4) needle valve; 5) pressure gauge for pressure measurement on the ceramic membrane; 6) valve open-close; 7) pressure chamber; 8) ceramic membrane; 9) vacuum pump; and 10) soap film flowmeter.

porosity (P_a) using the following equation [25]:

$$d_p = \left(\frac{150 k_D}{2.25 P_a}\right)^{0.5} \quad \text{(I)}$$

RESULTS AND DISCUSSION

The Al_2O_3 support showed low densification after sintering at 1300 ºC and reached only around 55% of relative density (Fig. 2). Increasing the PEG content, principally above 2 wt%, decreased considerably the supports' density ($\rho_r \cong 45.5\%$). The apparent porosity had a significant increase above 2 wt% PEG (14% to 46%, Fig. 2), following a behavior opposite to that observed for a relative density.

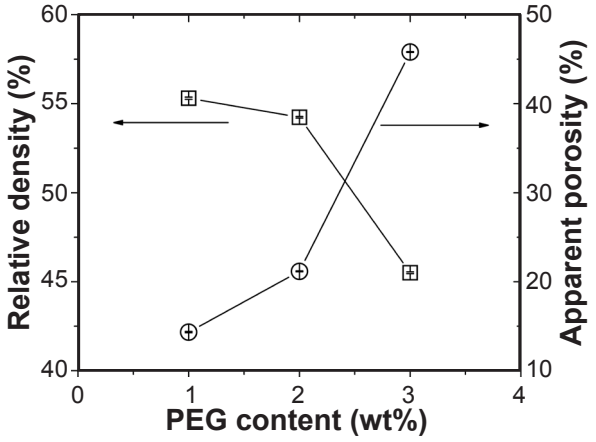

Figure 2: Relative density and apparent porosity as a function of PEG content added to the Al_2O_3 support.

Table I shows the porosity results of the Al_2O_3 support prepared with different PEG contents. The total porosity (P_t) had little variation (~10%) between 1 and 3 wt% PEG (Table I). However, the apparent (P_a) and closed (P_c) porosities exhibited significant variation for the same experimental condition (Table I). The increase in the PEG content caused a decrease from ~30% to ~9% in the fraction of closed pores in the Al_2O_3 support (Table I), which should improve the gas permeation by the porous support. All Al_2O_3 supports had microstructures with similar porous structures, regardless of the PEG content (Fig. 3). The pores were smaller than 1 μm with complex (tortuous) interconnectivity, like that usually observed in ceramic membranes for microfiltration produced by dry pressing [24].

Table I - Results of apparent (P_a), total (P_t), and closed (P_c) porosities of the Al_2O_3 supports.

PEG	P_a (%)	P_t (%)	P_c (%)
1%	14.34±0.07	44.69±0.06	30.36±0.07
2%	21.17±0.05	45.76±0.04	24.60±0.05
3%	45.80±0.04	54.50±0.05	8.70±0.04

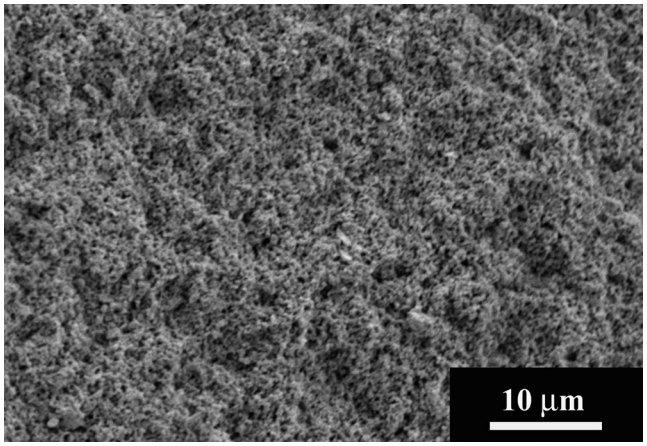

Figure 3: SEM image of the fracture surface of the Al_2O_3 support prepared with 3 wt% PEG.

The support's permeability was studied by the Darcy and Forchheimer models. According to Darcy's model (Eq. C), the permeability (k_D) showed an upward trend due to the increase in PEG content (Fig. 4a). This greater gas permeation was associated with the increase in apparent porosity (Pa, Table I) caused by the rise in the PEG content in the composition of the Al_2O_3 support. However, even with the increase in apparent porosity and the decrease in closed porosity (Table I), k_D had an irrelevant increase for additions above 2 wt% PEG (Fig. 4a). This minor rise in k_D was related to the low loss of viscous energy caused by the small variation in the pore size with the increase in PEG content, as reported in the literature [21]. Despite this, the gas permeability increases with the increase in the quantity of different pore-forming agents [poly(vinyl acetate), PVA, and polymethylmethacrylate, PMMA] added to ceramic membranes [20, 21, 24].

In order to analyze the effect of the pore structure on the gas permeability of the Al_2O_3 support, the Forchheimer model (Eq. D) was used, which makes it possible to investigate the inertial energy loss resulting from changes in the flux direction and fluid speed [24]. The Forchheimer's permeability (k_F, Fig. 4b) showed the same tendency as the Darcy permeability (k_D, Fig. 4a), showing an insignificant increase in k_F for additions above 2 wt% PEG. In this case, the inertial energy had a little variation because the pore size was almost unchanged above 2 wt% PEG, which resulted in a slight increase in the value of k_F. On the other hand, the increase in k_F between 1 and 2 wt% PEG was associated with the increase in open porosity, which favored the flow of CO_2 gas through the Al_2O_3 support. The Forchheimer number criterion (F_0) was used to determine the contributions of the viscous ($E_{viscous}$) and inertial ($E_{inertial}$) effects on the pressure drop of the fluid that permeated the porous material. The Eqs. F to H were used to calculate the values of F_0, $E_{viscous}$, and $E_{inertial}$, as shown in Table II. Even with a tortuous pore network (Fig. 3), F_0 was less than 1 (Table II), showing that the inertial effects had little influence on the pressure drop caused by permeation of CO_2 gas into the Al_2O_3 support ($E_{inertial}$<0.60%, Table II). Although the increase in

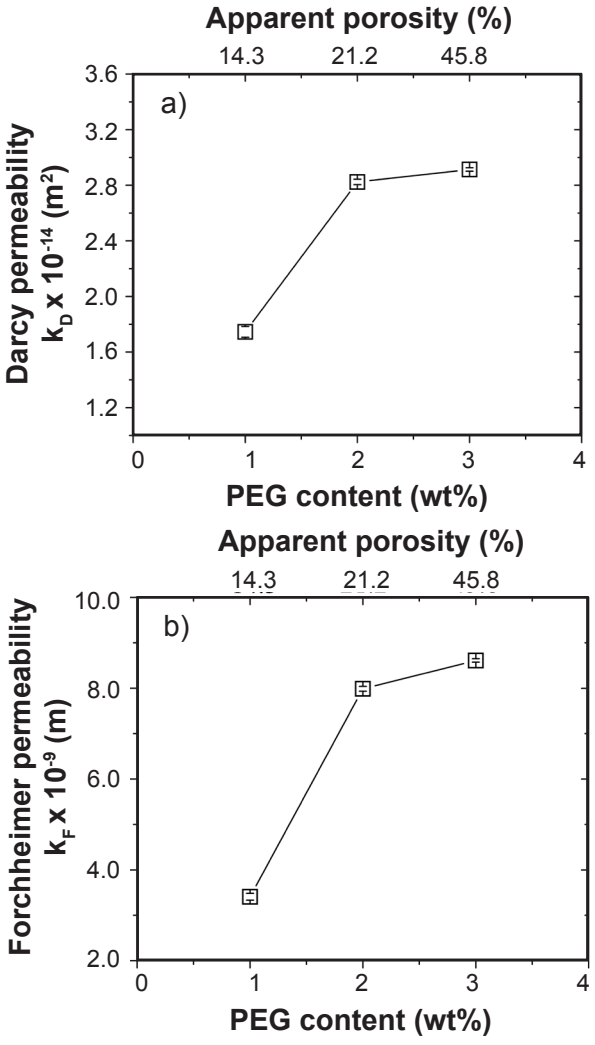

Figure 4: Darcy permeability (a) and Forchheimer permeability (b) as a function of the PEG content added to the Al_2O_3 support.

PEG content led to an augmentation in the fraction of the open pores and a diminution in the fraction of the closed pores (Table I), a small variation in morphology and pore size was observed by microstructural analysis. According to Eq. I, the average pore diameter (d_p) was below 1 μm for the three Al_2O_3 supports (Table II), agreeing with the microstructural analysis. The values of k_D and k_F were little influenced, mainly above 2 wt% PEG, because the estimated values for d_p were near for the samples with 1 to 3 wt% PEG. The tortuosity of the interconnected pore network was not intensified by the increase of PEG content, showing that the values of $E_{inertial}$ were low and relatively similar (Table II). Therefore, permeability behavior was influenced principally by viscous effects, which were reduced by the increase in pore size, since it favors the CO_2 gas flux through the Al_2O_3 support.

Table II - Number of Forchheimer (F_0), percentage of viscous effects ($E_{viscous}$), percentage of inertial effects ($E_{inertial}$), and average pore size (d_p) of the Al_2O_3 supports.

PEG	F_0 (x10^{-3})	$E_{viscous}$	$E_{inertial}$	d_p (μm)
1%	(5.67±0.12)	99.44%	0.56%	0.28±0.05
2%	(5.10±0.03)	99.49%	0.51%	0.29±0.05
3%	(5.03±0.02)	99.50%	0.50%	0.20±0.04

Fig. 5 shows a classification map of porous ceramic materials, which was constructed from the Forchheimer and Darcy permeabilities. In this paper, the ranges of k_F and k_D values were 3.4-8.6x10^{-9} m and 1.8-2.9x10^{-14} m^2, respectively. These results were plotted in Fig. 6 and, as seen, the Al_2O_3 supports with additions of 1 to 3 wt% PEG were classified as membranes for micro, ultra, and nanofiltration. As mentioned, the Al_2O_3 supports exhibited microstructures similar to those observed in microfiltration systems and, therefore, the developed device for permeability measurement may be used to characterize supports and membranes with low gas flux.

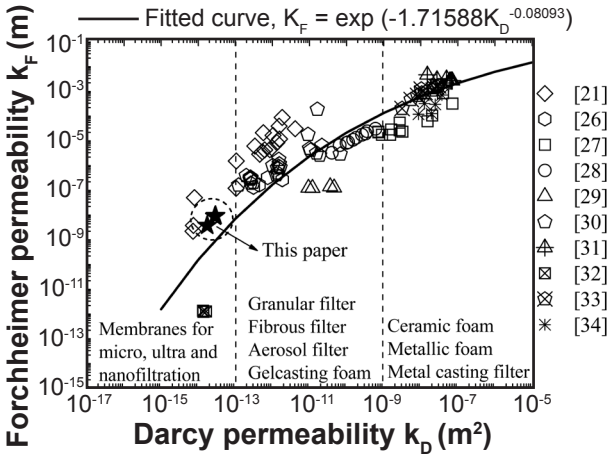

Figure 5: Classification map of porous ceramic materials constructed from the Forchheimer and Darcy permeabilities.

Fig. 6 shows the dependence of permeability and compressive strength with the porosity for the Al_2O_3 supports with different PEG contents. The compressive strength

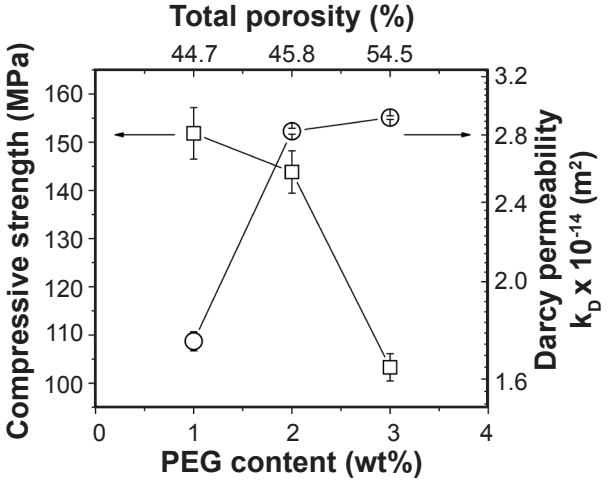

Figure 6: Compressive strength and Darcy permeability as a function of PEG content added to the Al_2O_3 support.

decreased from 152 to 103 MPa with the total porosity increasing from 44.7% to 54.5% (Fig. 6). Similar results were observed for different types of ceramic membranes [20, 25, 35]. This decline in the mechanical resistance as a function of porosity can be adjusted to numerous exponential and polynomial mathematical models [36]. An inverse behavior was observed for permeability (Fig. 6), showing that the increase in porosity improves the fluid permeation. That way, the two properties displayed antagonistic dependencies in relation to porosity. In this paper, an optimized condition was observed at 2 wt% PEG, in which the two properties presented high values [37].

CONCLUSIONS

Al_2O_3 supports were prepared by dry pressing, the addition of a pore-forming agent (polyethylene glycol, PEG), and partial sintering. An experimental apparatus was developed to study the permeability, measuring the pressure variation and the CO_2 gas flux that permeates the porous support. The open porosity increased as a function of the PEG content, but the average pore size remained almost unchanged. The permeability behavior was influenced by the increase in the fraction of open porosity, mainly between 14% and 21%. Above this porosity, the permeability had a slight variation because the values of pore size were relatively similar. The tortuosity of the interconnected pore network was not increased as a function of the PEG content since the inertial effects on the permeability behavior were low and relatively close between 1 and 3 wt% PEG. Thus, the permeability was affected mainly by viscous effects. The correlation between the Forchheimer and Darcy permeabilities indicated that the Al_2O_3 supports can be used in micro, ultra, and nanofiltration systems, showing that the developed device is feasible to characterize gas permeability in porous substrates or asymmetric ceramic membranes with low gas flux. Compressive strength and gas permeability exhibited antagonistic dependencies in relation to porosity, showing a compromise relationship between the two properties. For the experimental conditions of this work, an optimized condition was observed at 2 wt% PEG, in which the two properties achieved high values when analyzed in relation to porosity.

ACKNOWLEDGMENT

Thanks are due to IF Sudeste MG - Campus Juiz de Fora for supporting this research.

REFERENCES

[1] T. Arumugham, N.J. Kaleekkal, S. Gopal, J. Nambikkattu, R.K.A.M. Aboulella, S.R. Wickramasinghe, F. Banat, J. Environ. Manage. **293** (2021) 112925.
[2] W. Zhu, Y. Liu, K. Guan, C. Peng, J. Wu, J. Eur. Ceram. Soc. **39**, 4 (2019) 1712.
[3] X. Yin, J. Wu, P. Gao, K. Guan, C. Peng, Ceram. Int. **45**, 13 (2019) 16173.
[4] L.L. Coelho, M. di Luccio, D. Hotza, R.F.P.M. Moreira, A.C. Moreira, C.P. Fernandes, K. Rezwan, M. Wilhelm, J. Membr. Sci. **623** (2021) 119056.
[5] Z. Zhang, T.C.A. Ng, Q. Gu, L. Zhang, Z. He, Z. Lyu, X. Zhang, W. Wang, H.Y. Ng, J. Wang, J. Am. Ceram. Soc. **103**, 5 (2020) 3361.
[6] Q. Gu, T.C.A. Ng, W. Zang, L. Zhang, Z. Lyu, Z. Zhang, H.Y. Ng, J. Wang, J. Eur. Ceram. Soc. **40**, 15 (2020) 5951.
[7] X. Song, B. Jian, J. Jin, Ceram. Int. **44**, 16 (2018) 20366.
[8] E. Drioli, L. Giorno (Eds.), "Comprehensive membrane science and engineering", Elsevier, Kidlington (2010) 92.
[9] S.K. Hubadillah, M.H.D. Othman, T. Matsuura, A.F. Ismail, M.A. Rahman, Z. Harun, J. Jaafar, M. Nomura, Ceram. Int. **44**, 5 (2018) 4538.
[10] A.O. Silva, D. Hotza, R. Machado, K. Rezwan, M. Wilhelm, J. Eur. Ceram. Soc. **41**, 1 (2021) 871.
[11] S. Mestre, A. Gozalbo, M.M. Lorente-Ayza, E. Sánchez, J. Eur. Ceram. Soc. **39**, 12 (2019) 3392.
[12] T. Ohji, M. Fukushima, Int. Mater. Rev. **57**, 2 (2012) 115.
[13] D.F. Souza, E.H.M. Nunes, J.A. Queiroga, W.L. Vasconcelos, J. Eur. Ceram. Soc. **38**, 11 (2018) 4020.
[14] L.L.O. Silva, D.C.L. Vasconcelos, E.H.M. Nunes, L. Caldeira, V.C. Costa, A.P. Musse, S.A. Hatimondi, J.F. Nascimento, W. Grava, W.L. Vasconcelos, Ceram. Int. **38**, 3 (2012) 1943.
[15] W. Zhu, Y. Liu, K. Guan, C. Peng, W. Qiu, J. Wu, J. Eur. Ceram. Soc. **39**, 4 (2019) 1316.
[16] M. Issaoui, L. Limousy, C. R. Chim. **22**, 2-3 (2019) 175.
[17] N. Kamoun, W. Hajjeji, R. Abid, M.A. Rodriguez, F. Jamoussi, Cerâmica **66**, 380 (2020) 386.
[18] N. Ahmed, F.Q. Mir, Trans. Indian Ceram. Soc. **80**, 1 (2021) 41.
[19] S. Mestre, A. Gozalbo, M.M. Lorente-Ayza, E. Sánchez, J. Eur. Ceram. Soc. **39**, 12 (2019) 3392.
[20] Y. Li, X. Yang, D. Liu, J. Chen, D. Zhang, Z. Wu, Ceram. Int. **45**, 5 (2019) 5952.
[21] J. Kim, J.H. Ha, J. Lee, I.H. Song, Ceram. Int. **45**, 5 (2019) 5231.
[22] M.D.M. Innocentini, P. Sepulveda, F.S. Ortega, in "Cellular ceramics: structure, manufacturing, properties and applications", M. Scheffler, P. Colombo (Eds.), Wiley-VCH, Weinheim (2006) 313.
[23] I.S. Durazo-Cardenas, J. Corbett, D.J. Stephenson, Ceram. Int. **40**, 2 (2014) 3041.
[24] X. Li, D. Yao, K. Zuo, Y. Xia, J. Yin, H. Liang, Y.P. Zeng, J. Eur. Ceram. Soc. **39**, 9 (2019) 2855.
[25] L. Simão, R.F. Caldato, M.D.M. Innocentini, O.R.K. Montedo, Ceram. Int. **41**, 3 (2015) 4782.
[26] A. Dey, N. Kayal, O. Chakrabarti, M.D.M. Innocentini, W.S. Chacon, J.R. Coury, Int. J. Appl. Ceram. Technol. **10**, 6 (2013) 1.
[27] A.P. Philipse, H.L. Schram, J. Am. Ceram. Soc. **74**, 4 (1991) 728.
[28] A. Kumar, K. Mohanta, D. Kumar, O. Parkash,

Microporous Mesoporous Mater. **213** (2015) 48.
[29] A. Gómez-Martín, M.P. Orihuela, J.A. Becerra, J. Martínez-Fernández, J. Ramírez-Rico, Mater. Des. **107** (2016) 450.
[30] N. Gascoin, Int. J. Multiphase Flow **37**, 1 (2011) 24.
[31] M.D.M. Innocentini, V.R. Salvini, V.C. Pandolfelli, J.R. Coury, J. Am. Ceram. Soc. **82**, 7 (1999) 1945.
[32] H. Najmi, E. El-Tabach, K. Chetehouna, N. Gascoin, F. Falempin, Int. J. Hydrogen Energy **41**, 1 (2016) 316.
[33] Z. Wu, C. Caliot, F. Bai, G. Flamant, Z. Wang, J. Zhang, C. Tian, Appl. Energy **87**, 2 (2010) 504.
[34] S. Akbarnejad, M.S. Pour, L.T.I. Jonsson, P.G. Jönsson, Metall. Mater. Trans. B **48**, 1 (2017) 197.
[35] B.A. Latella, L. Henkel, E.G. Mehrtens, J. Mater. Sci. **41**, 2 (2006) 423.
[36] H.N. Yoshimura, A.L. Molisani, N.E. Narita, P.F. Cesar, H. Goldenstein, Mater. Res. **10**, 2 (2007) 127.
[37] P.C.F. Alves, D.G. da Silva, D.C.L. Vasconcelos, J.J. Vilela, J.F. do Nascimento, D.C. de Melo, W.L. Vasconcelos, Ceram. Int. **47**, 17 (2021) 24988.
(Rec. 28/06/2021, Rev. 19/08/2021, Ac. 31/08/2021)